Journal of Power Sources 196 (2011) 4791–4800

Contents lists available at ScienceDirect

Journal of Power Sources

journal homepage: www.elsevier.com/locate/jpowsour

Relationship between surface chemistry and electrochemical behavior of $LiNi_{1/2}Mn_{1/2}O_2$ positive electrode in a lithium-ion battery

Nicolas Dupré[a,*], Jean-Frédéric Martin[a,b], Julie Oliveri[a], Patrick Soudan[a,b], Atsuo Yamada[b], Ryoji Kanno[b], Dominique Guyomard[a]

[a] Institut des Matériaux Jean Rouxel, 2 rue de la Houssinière, BP 32229, F-44322 Nantes Cedex 3, France
[b] Department of Electronic Chemistry, Interdisciplinary Graduate School of Science and Engineering, Tokyo Institute of Technology, 4259 Nagatsuta, Midori, Yokohama 226-8502, Japan

ARTICLE INFO

Article history:
Received 31 May 2010
Received in revised form 9 July 2010
Accepted 18 July 2010
Available online 23 July 2010

Keywords:
Lithium batteries
Positive electrode
Interface
NMR

ABSTRACT

The formation and the evolution of lithium-containing species on the surface of grains of a layered 4 V material such as $LiNi_{1/2}Mn_{1/2}O_2$ along the electrochemical cycling have been followed using ^{7}Li MAS NMR, electrochemical impedance spectroscopy (EIS) and XPS. Materials displaying different specific surface areas and stored in different atmospheres have been investigated in order to study the influence of the surface/volume ratio and the influence of the initial surface state, respectively. It is shown that the presence of an initial interphase of Li_2CO_3 influences the electrochemical behavior of the electrode, emphasizing the importance of the history of the electrode prior cycling. ^{7}Li MAS NMR experiments performed upon cycling indicate the formation of interphase species in reduction and their partial removal in oxidation, indicating the dynamic character of the interphase upon cycling. Combined NMR, EIS and XPS experiments show the strong influence of the electrode/electrolyte interphase evolution on the electrochemical performance. Such results lead us to draw conclusions on the optimal storage conditions of layered 4 V materials for Li-ion batteries such as $LiNi_{1/2}Mn_{1/2}O_2$.

1. Introduction

Lithium-ion batteries show great promises in meeting the high power goals established for hybrid electric vehicles and energy storage devices because of their relatively high energy density and high power density [1–4]. The toxicity of cobalt and safety issues related to the use of $LiCoO_2$ has lead to an extensive research effort to find alternative cathode materials in lithium-ion rechargeable batteries. Recently, layer-structured lithium nickel manganese oxides such as $LiNi_{1/2}Mn_{1/2}O_2$ [5–12] or $LiNi_{1/3}Mn_{1/3}Co_{1/3}O_2$ [13–20] have been shown to be amongst the most promising candidates to replace $LiCoO_2$ due to their electrochemical and safety characteristics, which are more favourable than those of $LiCoO_2$. $LiCoO_2$ cost is twice that of $LiNi_{1-x}M_xO_2$ and approximately four times that of $LiMn_2O_4$ and although, based on the delivered energy positive electrode materials containing Ni or Mn are only 30% less expensive, production on a large scale makes Ni/Mn or iron phosphate materials very attractive. Following and monitoring the evolution of the electrochemical behavior of these materials along the electrochemical cycling and/or storage, represent an important step in the performance improvement process. It has been now demonstrated that the complex surface chemistry can be decisive in determining the long term viability of lithium transition metal oxides cathodes in terms of irreversible capacity loss, charge transfer kinetics and storage properties. To date, there have been several reports of electrode/electrolyte interphase formation on cathode materials, and recent evidence from electrochemical impedance [21–26], FTIR and XPS [27–29] showing that passivating films or species coming from the decomposition of the electrolyte are being formed on the cathode as a function of cycling and aging conditions. However, the experimental conditions of formation, growth and modification as well as the intimacy of the interactions between the surface layer and the surface of active material is still unclear [26,30–33]. In particular, the beneficial or hindering role played by the interphase(s) is yet to be addressed. Attempts to answer these issues are not a straightforward task due to experimental complications including the low amount of surface species that forms and the high sensitivity of the interphase towards ambient atmosphere.

MAS NMR has been proved to be an extremely powerful tool, able to probe both the bulk of the materials used as electrodes and the surface layers arising after contact with atmosphere or with the electrolyte of a lithium battery [34–38]. In this paper, we apply a combination of in situ electrochemical impedance spectroscopy (EIS), ex situ ^{7}Li MAS NMR technique and ex situ X-ray

* Corresponding author. Tel.: +33 2 40 37 39 33; fax: +33 2 40 37 39 95.
E-mail address: nicolas.dupre@cnrs-imn.fr (N. Dupré).

0378-7753/$ – see front matter © 2010 Elsevier B.V. All rights reserved.
doi:10.1016/j.jpowsour.2010.07.049

photoelectron spectroscopy (XPS) to examine the surface reactivity, interphase formation and the evolution of lithium-containing species on the surface of grains of layered $LiNi_{1/2}Mn_{1/2}O_2$ along cycling in a lithium battery. We focus our studies on the comparison of materials stored under ambient atmosphere or argon in order to follow the influence of the initial surface chemistry on their subsequent surface and electrochemical behavior.

2. Experimental

The $LiNi_{1/2}Mn_{1/2}O_2$ samples used for this study have been obtained through the classic coprecipitation method, followed by annealing at 1000 °C as described elsewhere [5,6]. A second synthesis method through a combustion route involving glycine, followed by annealing at 950 °C, has been employed [39]. For both syntheses, half of the batch was directly transferred into an argon glovebox and the other half stored in a closed (but not air tight) vial outside the glovebox.

XRD data were collected with a $\theta/2\theta$ BRUKER D5000 diffractometer ($\lambda_{Cu\,K\alpha}$) equipped with a linear MOXTEK detector, using a scan step of 0.01° (2θ) for 10 s.

Galvanostatic cycling was performed using Swagelok cells and MacPile system at a C/10 rate. A slurry of the electrode powder in n-methyl-pyrolidinone (NMP) was deposited on a 1 cm^2 aluminum disk and then dried under vacuum at 100 °C for 24 h. Electrodes were constituted of 75 wt% of active material, 20 wt% of ketjenblack carbon and 5 wt% poly-vinylidene di-fluoride (PVdF). Masses of active material were typically 8–10 mg. To facilitate the recovering of samples for XPS and NMR studies, electrodes were not pressed prior to cycling. Batches of 3–5 cells have been cycled in order to insure reproducibility of the cycling behavior. The polarization was determined as the difference between the charge and discharge peaks in the incremental capacity curves derived from galvanostatic data.

Electrochemical impedance spectroscopy (EIS) measurements (from 10 mHz to 200 kHz) were obtained using a VMP/Z apparatus (Bio-logic, France). A home-made Swagelok-type three electrodes cell was used. The negative electrode was made of a disk of lithium metal. The reference electrode consists of a ring of lithium metal surrounding the working electrode. Measurements have been performed at the end of a 5 h relaxation rest upon discharge down to 2.5 V and upon charge up to 4.5 V for different C/10 galvanostatic cycles at ambient temperature. The samples made for NMR have been obtained after 1, 5 and 20 electrochemical cycles. Cells were cycled in galvanostatic mode at C/10 rate and a subsequent stabilization at the end of charge (4.5 V) or the end of discharge (2.5 V) using a constant potential step for 100 h.

^{7}Li NMR measurements were carried out at room temperature on a Bruker Avance-500 spectrometer (B_0 = 11.8 T, Larmor frequency ν_0 = 194.369 MHz in ^{7}Li resonance). Single-pulse MAS spectra were obtained by using a Bruker MAS probe with a cylindrical 4-mm o.d. zirconia rotor. Spinning frequencies up to 14 kHz were used. A short single-pulse length of 1 μs corresponding to a non-selective $\pi/2$ pulse was applied. Recycle time was in the 0.5–60 s range and a spectrometer dead time (preacquisition delay) of 4.5 μs was used before each acquisition. The isotropic shifts, reported in parts per million (ppm), are relative to an external liquid 1 M solution of LiCl set at 0 ppm. Isotropic resonances were identified using variable spinning speed. In order to perform a quantitative analysis, the different spectra have been analyzed considering the total integrated intensity of the signal for each sample. Of course, all parameters were kept constant for each series of NMR measurements: number of scans, probe tuning process, spinning frequency, etc. The spectra displayed in this work were normalized taking into account the number of scans and the mass of sample. In the case of the comparison of materials with different specific surfaces, NMR signals were, in addition, normalized to the specific surface area.

X-ray photoelectron spectroscopy (XPS) data have been collected after different cycle numbers using a Kratos Ultra Axis spectrometer. The X-ray source is AlK working at 1253.6 eV and the spot size is 0.7 × 0.3 mm. A special air-tied sample holder has been used to transfer the samples from the glove box to the spectrometer, in order to avoid any reaction with ambient atmosphere. Semiquantitative XPS analysis has been performed using pseudo-Voigt function constrained by full width at half-maximum (FWHM) ranges typical of each element. The validity of the analyses was confirmed by an experimental M/O ratio close to the theoretical one for the bare pristine compound. Binding energies were fixed at ±0.2 eV of the given value. The nickel contribution, overlapping with fluorine contribution was not taken into account.

3. Results

3.1. Physico-chemical and electrochemical characterizations

XRD characterization of bulk $LiNi_{1/2}Mn_{1/2}O_2$ synthesized by coprecipitation and combustion methods is detailed elsewhere [38]. Diffraction patterns for $LiNi_{1/2}Mn_{1/2}O_2$ samples obtained through the two chosen synthesis routes are similar. No impurity was detected and the X-ray diagrams were indexed and refined in the *R*-3*m* space group with a single phase. The lattice parameters *a* and *c* were 2.891(1) and 14.32(1) Å, respectively, for the coprecipitation method and 2.889(1) and 14.29(2) Å for the combustion method, which are close to the reported data (2.89 and 14.30 Å, respectively [6]). The Rietveld refinement yielded crystallite sizes respectively of 174.6 and 139.5 nm, for the coprecipitation and combustion method. The Rietveld refinement of the diffracted intensities was also consistent with the already reported 10% exchange of Li and Ni between lithium layers and metal transition layers [6]. In addition, XPS indicated the presence of Li_2CO_3 on the surface of grains of active material that have been stored in ambient atmosphere while Li_2CO_3 is absent from the surface of the materials stored in argon [36,38]. In addition, specific surface area measurements done by BET method yielded values of 4 and 8 $m^2\,g^{-1}$ for the coprecipitation and the combustion routes, respectively. Grain sizes, estimated from routine SEM experiments are 300 and 120 nm for the coprecipitation and the combustion routes, respectively. The different characteristics of the pristine samples are summarized in Table 1.

The specific capacity curves for samples obtained by the two chosen synthesis routes and further stored in argon or in ambient atmosphere, are displayed in Fig. 1. Whatever their different morphologies and surface areas coming from different synthesis routes,

Table 1
Pristine interphase as a function of synthesis conditions, BET values and storage conditions for $LiNi_{1/2}Mn_{1/2}O_2$ samples.

Sample	Synthesis conditions	BET surface area (m^2/g)	Storage conditions	Initial surface layer
LMN-1	Combustion [40]	8	Argon	No layer
LMN-2	Combustion [40]	8	Air	Li_2CO_3
LMN-3	Coprecipitation [5,6]	4	Argon	No layer
LMN-4	Coprecipitation [5,6]	4	Air	Li_2CO_3

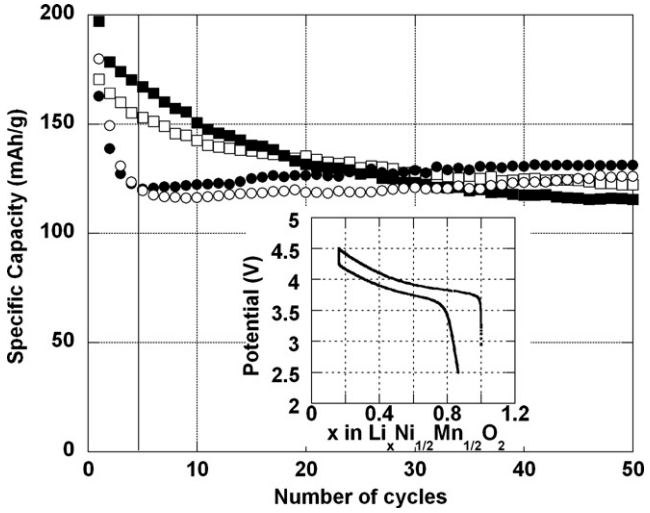

Fig. 1. Specific capacity curves for LMN-1 (white squares), LMN-2 (white dots), LMN-3 (black squares) and LMN-4 (black dots). Inset: voltage versus composition curve for the first cycle of LMN-3.

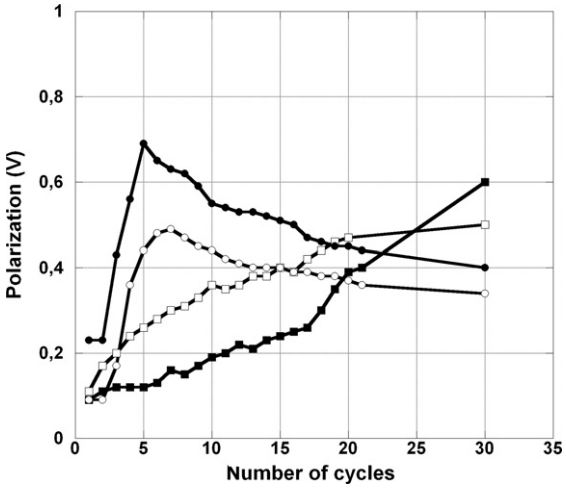

Fig. 2. Evolution of the peak-to-peak polarization as a function of the number of cycles for LMN-1 (white squares), LMN-2 (white dots), LMN-3 (black squares) and LMN-4 (black dots).

$LiNi_{1/2}Mn_{1/2}O_2$ samples display clearly different cycling behaviors, depending on the storage atmosphere. When $LiNi_{1/2}Mn_{1/2}O_2$ is stored under ambient atmosphere (LMN-2 and LMN-4), a fast and important capacity loss is exhibited along the five first cycles. A slow increase of the specific capacity is observed for the following cycles. On the other hand, for the samples stored under argon (LMN-1 and LMN-3), the initial capacity is larger but a continuous capacity loss upon cycling is noticed. It is well known that chemical history of the sample, in particular the heat treatment at high temperature [40] can lead to subtle changes in the cationic distribution in the transition metal layers that can influence the electrochemical performance. Nevertheless, even having slightly different cationic distribution due to different synthesis route, $LiNi_{1/2}Mn_{1/2}O_2$ obtained from combustion and $LiNi_{1/2}Mn_{1/2}O_2$ obtained from coprecipitation exhibit a similar evolution depending on their storage, which seems to be the driving parameter in the scope of the present study. The specific capacities, although slightly lower than reported in previous studies [9,10] on 4 V layered materials, stays in the same order of magnitude. The observed discrepancies probably come from the synthesis conditions used here that might lead to different cationic distribution. The nickel and manganese distribution in the transition metal layers is hardly detectable using a laboratory XRD equipment but these subtle changes can lead to changes in terms of specific capacity [40].

Similar differences appear concerning the evolution upon cycling of the polarization between charge and discharge (Fig. 2). The polarization typically includes both ohmic information (i.e. due to the growth of a superficial layer for instance) and kinetic information coming from both bulk insertion kinetics and interfacial kinetics at the electrolyte/electrode interface. The evolution is quite different depending on the storage atmosphere of the samples (Fig. 2). Indeed, samples obtained through the same synthesis route but stored in different atmospheres, and therefore showing identical bulks and different surface characteristics, exhibit different evolution of their polarization. It indicates that the evolution of the polarization observed for these samples reflects changes that occurred at the surface of grains of active material upon storage under different atmosphere. For LMN-1 and LMN-3, the polarization increases continuously showing a progressive deterioration of the intercalation/deintercalation kinetics at the electrode/electrolyte interface. On the contrary, concerning the samples stored in ambient atmosphere, the polarization reaches a maximum at the 5^{th} and 7^{th}, respectively for the LMN-4 and LMN-2, followed by a slow decrease. The polarization maxima correspond clearly to the change of behavior observed on the specific capacity curves (marked by a vertical solid line in Fig. 1).

Recently, it has been proved that Li_2CO_3 additive in the electrolyte neutralizes acidic species and prevents the degradation of $LiFePO_4$ electrodes from contact with $LiPF_6$-based electrolyte contaminated with water [41]:

$$LiPF_6 + H_2O \rightarrow LiF + 2HF + POF_3 \quad (1)$$

$$POF_3 + ne^- + nLi^+ \rightarrow LiF + Li_xPO_yF_z \quad (2)$$

$$Li_2CO_3 + 2HF \rightarrow 2LiF + H_2CO_3 \quad (3)$$

A similar phenomenon could take place in our case at the Li_2CO_3-recovered surface, leading to an acid–base reaction of the surface layer, and to a subsequent protection of the material laying underneath this surface layer and therefore to a more efficient passivation. The $LiPF_6$ (1 M in EC/DMC) electrolyte used for cycling experiments has been titrated at only 11 ppm of water using Karl Fischer coulometry. This suggests that although the scavenging of the acidic traces of the electrolyte by surface Li_2CO_3 is possible, it is not probably the only cause of the difference in performance between samples stored in argon and samples stored in ambient atmosphere, as we discuss below.

These results emphasize the importance of the chemical history of the surface of the electrode material before any electrochemical cycling and the strong correlation between interface phenomena and the electrochemical behavior. The origin of the different electrochemical behaviors upon cycling, both capacity and polarization could come from a different evolution of the positive electrode/electrolyte interphase due to different pristine surface chemistry. It becomes then crucial to look at the evolution of the interphase along the electrochemical cycling of the electrode, in particular as a function of the state of charge or discharge and the number of cycles. In the following, the detailed study is focused on two differently behaving $LiNi_{1/2}Mn_{1/2}O_2$ samples over the 20 first cycles, LMN-1 being stored in argon and LMN-4 being stored in ambient atmosphere.

3.2. ^{7}Li MAS NMR studies

^{7}Li MAS NMR spectra of air-stored LMN-4 electrodes at different cycling steps are displayed in Fig. 3. We decided to acquire NMR spectra after one full electrochemical cycle was completed to avoid any transitory regime occurring during the first cycle. Thus,

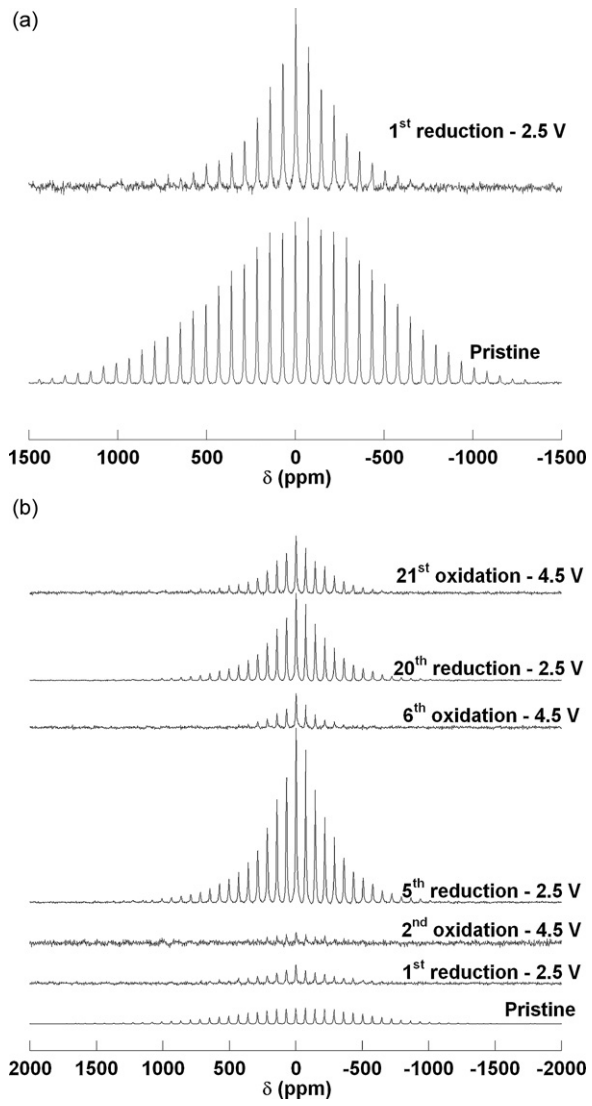

Fig. 3. (a) Normalized ^{7}Li MAS NMR spectra for pristine LMN-4 and at the end of the first discharge. (b) Normalized ^{7}Li MAS NMR spectra for LMN-4, at the end of 1st, 5th, 20th discharge, and 2nd, 6th, 21st charge.

spectra were acquired at the end of the first, fifth, twentieth discharge at 2.5 V and their respective subsequent charges at 4.5 V. As a remark, it is important to keep in mind that only the diamagnetic lithium is detected during these NMR experiments and that lithium inserted in the structure of the paramagnetic $LiNi_{1/2}Mn_{1/2}O_2$ is not observed under our experimental conditions [36]. Based on differences in relaxation times for Li in $LiNi_{1/2}Mn_{1/2}O_2$ (few μs) and Li in diamagnetic surface species (approximately 10–100 μs), waiting an appropriate delay between the NMR pulse and acquisition allows the signal of bulk Li to decay completely while the signal of surface species is still observable. The intensity detected does not depend on the amount of lithium ions present in the host matrix, but it depends quantitatively on the amount of lithium species on the surface of the active material [36]. All spectra exhibit one apparent isotropic resonance close to 1.5 ppm, which is in the range of diamagnetic lithium. The evolution of the interphase is not straightforward when first looking at the spectra (Fig. 3a and b). Nevertheless, several interesting points can be drawn. First, the ^{7}Li MAS NMR signal is clearly less intense after the first cycle compared to the pristine sample, confirming the dissolution, at least partially, of the initial Li_2CO_3. The slight change in the chemical shift from 2 to 1.5 ppm is consistent with the disappearing of the major part of

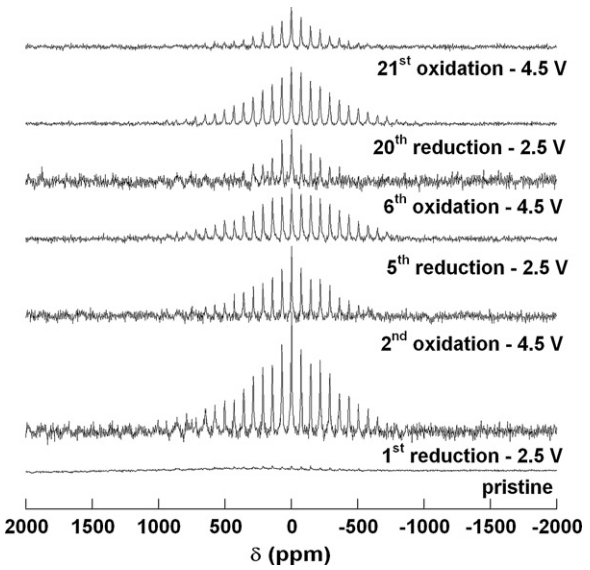

Fig. 4. Normalized ^{7}Li MAS NMR spectra for LMN-1, at the end of 1st, 5th, 20th discharge, and 2nd, 6th, 21st charge.

Li_2CO_3 and its replacement by other lithium-containing products. The observed chemical shift did not further change along the electrochemical cycling. A much narrower line shape can be observed for NMR spectrum after the first reduction compared to that of the pristine sample (Fig. 3a). An extremely strong dipolar interaction between the nuclear spins of lithium and the electronic spin of unpaired electrons dominates our spectra [36] and therefore, the observed narrowing is attributed to a weaker overall dipolar interaction between the observed lithium nuclei in the interphase and paramagnetic centres of the electrode material. As the dipolar interaction has a $1/r^3$ dependency (with r being the distance between two interacting spins), it suggests an overall lower degree of intimacy between part of the interphase and the surface of active material, showing a global architectural difference after an electrochemical cycle. The integrated intensity of the cycled sample (Fig. 3a) being lower and the line shape being narrower, it can be said that the proximity/intimacy of the detected surface layer to the bulk particles has decreased. In the case of a higher integrated intensity, the change in the line shape could have been assigned to a simple stacking of additional surface species exhibiting weaker interaction with the paramagnetic material.

Second, the ^{7}Li MAS NMR signal is always more intense at the end of discharge than at the end of the subsequent charge. Third, considering the samples recovered at high potential, the integrated intensity increases with the number of cycles. These results demonstrate the formation of lithium-containing surface species at low voltage and their partial removal at high voltage with an inherent accumulation along the electrochemical cycling. It demonstrates in particular that the interphase is a dynamic system which evolves along the cycling process. The integrated intensity maximum at the 5th cycle will be discussed in the discussion part.

The evolution of the interface for LMN-1 is depicted in Fig. 4. First of all, as observed for an air-stored sample (LMN-4), the intensity of the NMR signal is always more intense for a sample stabilized at the end of discharge compared to the end of charge, confirming the process of formation of surface species at low voltage and their partial destruction at high voltage. Then, this phenomenon does not depend on the storage atmosphere of the electrode prior to cycling but shows rather the influence of the potential on the interphase.

In the case of LMN-1, the NMR intensity after 1, 5 and 20 cycles (Fig. 4) evolves quite differently compared to air-stored LMN-4 sample, since the maximum of intensity is noticed for

Table 2
Quantitative analysis of XPS peaks observed for LMN-4 at the end of 1st, 5th, 20th discharge, and 2nd, 6th, 21st charge.

	Binding energy	Attributed species	1st red 2.5 V	2nd ox 4.5 V	5th red 2.5 V	6th ox 4.5 V	20th red 2.5 V	21st ox 4.5 V
C1s	284.6 eV	ketjen-black	30%	17%	18%	20%	23%	20.5%
	285.1 eV	Polycarbonates Li alkyl carbonates	22%	29.5%	37.5%	34%	26.5%	25%
	286.6 eV	PVdF	9.5%	21%	10%	13%	13%	8.5%
	289.3 eV	Polycarbonates Li alkyl carbonates	3%	5.5%	5%	5%	4%	3%
	290.5 eV	PVdF	5%	3.5%	2.5%	3.5%	3.5%	4.5%
O1s	529.5 eV	$LiNi_{1/2}Mn_{1/2}O_2$	0.5%	1%	0.5%	1.5%	0.5%	1.5%
	531.5 eV	Polycarbonates Li alkyl carbonates	1%	4.5%	1%	2%	1.5%	2.5%
	532.8 eV	Polycarbonates Li alkyl carbonates	3%	4.5%	6%	5%	3.5%	2.5%
	534.2 eV	Polycarbonates Li alkyl carbonates	2.5%	5%	5.5%	4.5%	3.5%	2.5%
F1s	685.2 eV	LiF	4%	1.5%	2%	0.5%	3%	1.5%
	687.5 eV	Li_xPF_y, $Li_xPO_yF_z$, PVdF	13%	4%	8.5%	7.5%	10%	12%
P2p	134.5 eV	$Li_xPO_yF_z$	0.5%	1%	0.5%	0.4%	0.4%	0.4%
	136.5 eV	Li_xPF_y,	0%	0%	0%	0.1%	0.1%	0.1%
Mn2p	642.5 eV	$LiNi_{1/2}Mn_{1/2}O_2$	0.5%	1%	0.25%	1%	0.5%	0.5%
Li1s	56 eV	LiF	4%	1.5%	3.5%	1%	4%	3%
	58 eV	Li_xPF_y, $Li_xPO_yF_z$	1.5%	0%	1%	0%	2%	2%

the ^{7}Li NMR spectrum corresponding to the reduced state (2.5 V) of the electrode at the end of the first discharge. The intensity then decreases significantly for the subsequent oxidation. A further slower decrease occurs at the 5th and 20th cycle for both 2.5 and 4.5 V samples. The overall decrease in the integrated NMR intensity suggests a progressive destruction of the interphase upon cycling as opposed to the behavior of the air-stored sample.

3.3. XPS studies

XPS measurements have been performed on LMN-1 and LMN-4 samples at the end of the first, fifth, twentieth discharge at 2.5 V and their respective subsequent charges at 4.5 V, in order to check the composition of the interphase. Quantitative data obtained from the analysis of the XPS peaks are given in Tables 2 and 3 for LMN-4 and LMN-1, respectively. The C1s peak at 284.6 eV is mostly due to the ketjen-black carbon of the composite electrode [26,42]. Characteristic C1s peaks of PVdF can be observed at 286.6 and 290.5 eV as well as F1s peak at 687.5 eV. The latter can overlap binding energies assigned to Li_xPF_y and $Li_xPO_yF_z$. Amounts of ketjen-black and PVdF were kept constant for all electrodes. The variation in percentage of their corresponding C1s and F1s contribution is attributed to their variable covering by other products. The O1s peak at 529.5 eV and the Mn2p peak at 642.5 eV correspond to the $LiNi_{1/2}Mn_{1/2}O_2$ oxide. Products identified in previous papers after a simple contact with the electrolyte, such as LiF (F1s at 685.2 eV and Li1s at 56 eV [43]), Li_xPF_y (Li1s at 58 eV and P2p at 136.5 eV) and $Li_xPO_yF_z$ (Li1s at 58 eV and P2p at 134.5 eV) are revealed by their characteristic lithium, phosphorus and fluorine peaks. Amounts of species included on the surface of the active material clearly exhibit differences with respect to the number of cycles and potential confirming that the interphase evolves along the electrochemical cycling and therefore is not a static system. The same inorganic species are involved in the interphase along the electrochemical cycling with amounts of LiF being always larger at the end of reduction for both materials. C1s and O1s spectra display contributions at 285.1, 289.3 eV, and 531.5, 532.8, 534.2 eV, respectively, indicating the presence of organic species such as polycarbonates and lithium alkyl carbonates already detected in previous studies [44–46].

Concerning LMN-4, during the first oxidation, the percentage of carbon attributed to polycarbonates and alkyl carbonates (285.1 and 289.3 eV) increases. It indicates an increasing coverage of the surface of the electrode by organic species. This result is confirmed by the increase of the contribution of oxygen at (531.5, 532.8 and 534.2 eV). The decrease of the contribution from other elements supports this trend.

Table 3
Quantitative analysis of XPS peaks observed for LMN-1 at the end of 1st, 5th, 20th discharge, and 2nd, 6th, 21st charge.

	Binding energy	Attributed species	1st red 2.5 V	2nd ox 4.5 V	5th red 2.5 V	6th ox 4.5 V	20th red 2.5 V	21st ox 4.5 V
C1s	284.6 eV	Ketjen-black	15%	15%	14.5%	21.5%	21.5%	21%
	285.1 eV	Polycarbonates Li alkyl carbonates	25.5%	30.5%	31%	29%	30%	30%
	286.6 eV	PVdF	11.5%	12%	14%	10%	10%	9%
	289.3 eV	Polycarbonates Li alkyl carbonates	4.5%	4.5%	4.5%	4.5%	4%	3.5%
	290.5 eV	PVdF	4.5%	5%	4%	4.5%	5%	5%
O1s	529.5 eV	$LiNi_{1/2}Mn_{1/2}O_2$	0.5%	2%	1%	2.5%	1%	3%
	531.5 eV	Polycarbonates Li alkyl carbonates	2.5%	2.5%	2%	4%	5%	3.5%
	532.8 eV	Polycarbonates Li alkyl carbonates	4%	5%	3.5%	3%	2.5%	4.5%
	534.2 eV	Polycarbonates Li alkyl carbonates	2.5%	5%	3%	2.5%	2.5%	4%
F1s	685.2 eV	LiF	8.5%	4.5%	3.5%	2%	3%	3%
	687.5 eV	Li_xPF_y, $Li_xPO_yF_z$, PVdF	11.5%	11.5%	11.5%	12%	10%	10.5%
P2p	134.5 eV	$Li_xPO_yF_z$	0.5%	0.5%	0.25%	0.3%	0.5%	0.5%
	136.5 eV	Li_xPF_y,	0%	0%	0.25%	0.2%	0%	0%
Mn2p	642.5 eV	$LiNi_{1/2}Mn_{1/2}O_2$	0.5%	1.25%	1%	1.5%	1%	1.5%
Li1s	56 eV	LiF	4.5%	3%	2.5%	3%	3%	2%
	58 eV	Li_xPF_y, $Li_xPO_yF_z$	4%	0%	3%	0%	2%	0%

For the 5th reduction, contribution from C–C and C–H bonds (C1s at 285.1 eV) clearly increases, the fluorine signal (F1s at 685.2 eV) decreases and the contribution of the manganese becomes extremely low, reaching its minimum. It indicates a maximum in the covering of the electrode material by the interphase species. The decrease in the percentage of fluorine and lithium assigned to LiF reflects then its covering by organic species rather than a removal of lithiated inorganic species at the end of discharge.

Concerning the 6th oxidation, the decrease in the contributions from all interphase species (C1s at 285.1 eV, O1s at 532.8 and 534.2 eV, Li1s at 56 and 58 eV and F1s at 685.2 eV) to the benefit of contributions from manganese, PVdF and carbon black is consistent with a partial removal of the interphase in agreement with the evolution observed by NMR.

For the 20th cycle, the contribution of carbon due to polycarbonates and alkyl carbonates (285.1 eV) has slightly decreased and the percentage of Li attributed to LiF has globally increased compared to the 5th cycle, consistent with a less substantial covering of the surface by organic species making inorganic surface species more visible. The overall evolution of the detected amount of surface organic products follows a similar trend to what is observed by NMR.

Concerning LMN-1, after the first reduction, larger amounts of lithium assigned to LiF and $Li_xPF_y/Li_xPO_yF_z$ can be observed compared to samples further cycled. The contribution of manganese is also the lowest at the end of the first reduction, consistent with a more substantial covering of the active material surface by the interphase at the early stage of the electrochemical cycling. The interphase Li contributions then decrease along the electrochemical cycling. The 20th cycle shows no difference with the 5th cycle and a more monotonous evolution of the interphase composition upon cycling can be deduced for LMN-1, which also is in agreement with the slow and progressive evolution observed using NMR for the argon-stored sample.

3.4. EIS studies

In order to gather information on the phenomena taking place at the interface, we performed in situ electrochemical impedance spectroscopy (EIS) measurements with three electrodes cells, at ambient temperature. Fig. 5 displays the Nyquist plots for electrodes stored in air (a) and in argon (b) stabilized at the end of the 1st, 5th 20th discharges and their subsequent charges. For each tested electrode, the Nyquist diagram exhibits one semicircle at high frequency from which a capacitance in the range 10–20 μF cm^{-2} can be calculated, depending on the sample. It corresponds to the typical order of magnitude of double layer capacitance. In order to rule out the hypothesis of a solid resistive layer (SEI) covering completely the electrode surface, measurements have been done, at higher temperature (60 °C) [37]. A decrease in the resistance of the semi-circle and a stable capacitance was clearly observed and lead us to assign the corresponding phenomenon to a charge transfer process. Consequently, this semicircle is attributed to a charge transfer resistance in parallel with a double layer capacitance. However, we cannot exclude a minimum contribution (non-measurable) of possible resistive surface layer [42]. In order to be as general as possible, the resistance measured on the Nyquist plots will be called interfacial resistance in the following. Concerning LMN-4, the resistance measured at the end of discharge passes through a clear maximum after 5 cycles before decreasing during further cycling. The resistance measured at the end of charge increases between the first and 5th cycle whereas no significant evolution could be noticed between the 5th and the 20th cycle. For LMN-1, a different behavior can be observed (Fig. 5b), with only a progressive increase of resistance measured at the end of reduction from the first to the 20th cycle. As opposed to the case of LMN-4 reaching stabilization after the 5th cycle, the resistance measured at the end of charge increases significantly between the 5th and the 20th the cycle, indicating a growing deterioration of interfacial processes. This behavior is further analyzed in the discussion part.

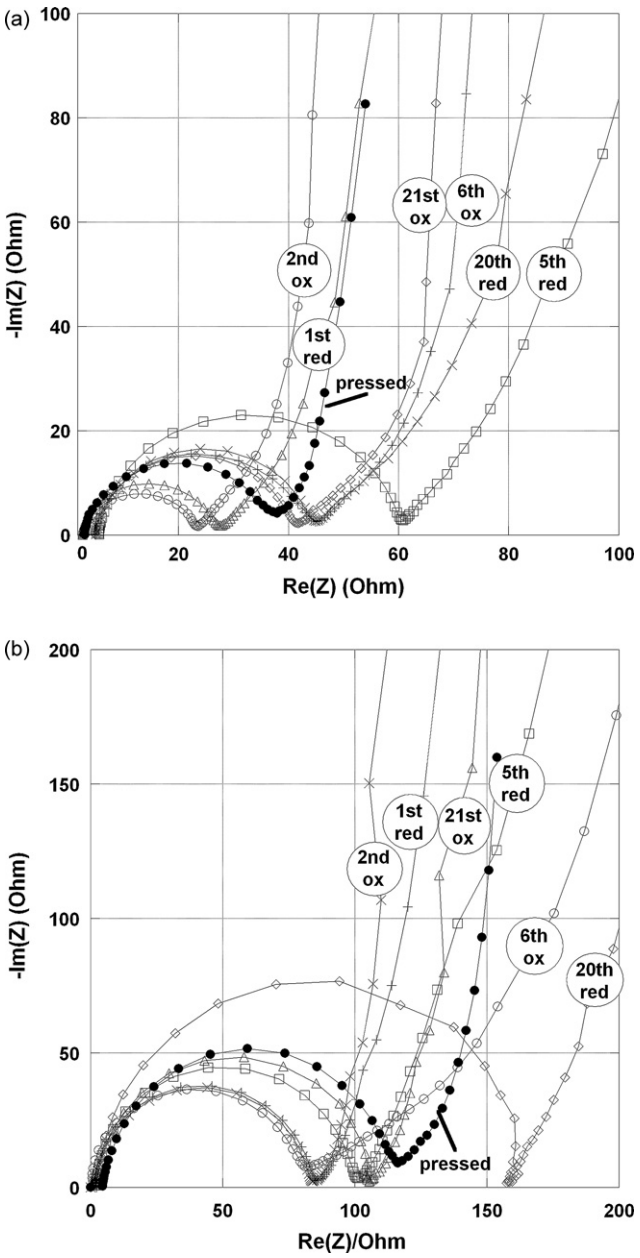

Fig. 5. Nyquist diagrams for LMN-4 (a) and LMN-1 (b), at the end of 1st, 5th, 20th discharge, *d* 2nd, 6th, 21st charge and after being pressed under 3 tons after the 20th discharge.

4. Discussion

4.1. Relationships between surface chemistry and electrochemical behavior

Fig. 6 gathers and summarizes the main data already presented in order to get some comparative overview of the very important aspects of the interphase evolution.

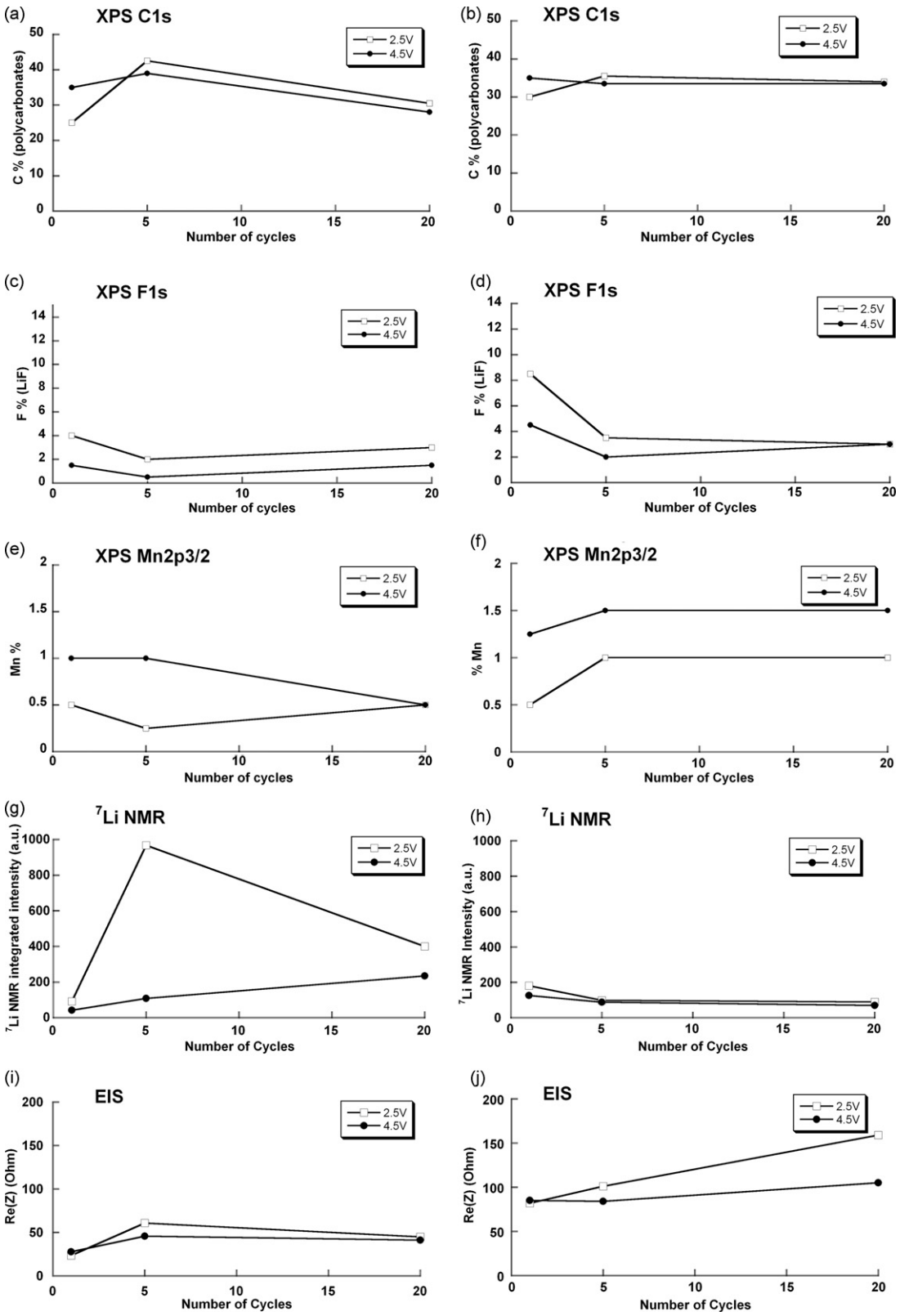

Fig. 6. Comparative overview of interphase evolution for LMN-4 and LMN-1, respectively, expressed as integrated intensities for XPS C1s (a and b), F1s (c and d), Mn2p3/2(e and f) peaks, integrated ^{7}Li NMR intensity normalized to the mass of sample and specific surface (g and h) and interfacial resistance (i and j), at the end of discharge (white dots), at the end of charge (black dots). C1s contribution from PVDF (286.6 and 290.5 eV), pollution carbon and carbon black (284.6 eV) as well as and F1s peak at 687.5 eV which includes contribution from PVdF have not been taken into account.

For air-stored LMN-4 sample, the variation of the specific discharge capacity with the cycle number shows a sharp decrease up to the 5th cycle and then a slight increase (Fig. 1). Simultaneously, polarization (Fig. 2), surface ^{7}Li NMR intensity in reduced state (Fig. 3 and Fig. 6g) and interfacial resistance in reduced state (Fig. 5 and Fig. 6i) display a sharp increase up to the 5th cycle and then a slower decrease for higher cycle numbers. Such clear correlation between the evolution of these different data upon cycling has been already analyzed in our previous paper [37]. The correlation between surface phenomena (amount of interface species calculated from surface Li NMR intensity and difficulty to cross the interface, possibly due to a restrained accessible surface due to these interface species, deduced from interfacial resistance determined from EIS) and electrochemical bulk properties (total capacity, and overall kinetics obtained from polarization) has been emphasized, and lead us to conclude for a unique control by surface phenomena of the overall electrochemical behavior.

In the present paper, XPS data have been added, which give complementary information on the chemical nature of the surface species involved. The nature of the species present in the interphase does not change along the electrochemical cycling. It can be observed that the opposite evolution of the $LiNi_{1/2}Mn_{1/2}O_2$Mn2p3/2 and polymeric carbonates/Li alkyl carbonates C1s contributions at the end of discharges is in agreement with a covering of the surface that is maximum for the 5th reduction although the variations along the electrochemical cycles are not as important compared to the NMR data (Fig. 6a and e). The evolution of the amount of LiF (Fig. 6c) is in apparent contradiction with the evolution of lithiated species deduced from NMR data and shows also an opposite evolution compared to Mn2p3/2 and polymeric carbonates/Li alkyl carbonates C1s contributions. It suggests that organic species cover also the inorganic lithiated and fluorinated species. The interphase observed in our samples can be considered as LiF, as well as other inorganic decomposition products coming from the decomposition of $LiPF_6$, within an organic matrix made of decomposition products of electrolyte solvents.

The evolution of the interphase is different in the case of Ar-stored LMN-1 sample. Contrasting with the behavior of air-stored LMN-4 sample, an important increase of the interfacial resistance can be observed on the EIS spectra (Fig. 6i and j) upon cycling. The evolution of the interfacial resistance correlates well with the continuous decrease of the specific capacity (Fig. 1) and the continuous increase of the peak-to-peak polarization (Fig. 2). Such data show deterioration of the overall kinetics.

Nevertheless, the slow decrease of the NMR integrated intensity noticed from the 1st to the 20th cycle, does not seem at first sight compatible with an interface degradation. The observed evolution rather indicates a progressive removal of the surface lithiated species. An overall decrease in the surface species is also suggested by XPS as the percentage of visible manganese is slightly higher after 20 cycles compared to the first cycle (Fig. 6f). In this case, the degradation of the electrochemical performance cannot be linked directly to the evolution of the amount of interphase species since they show opposite variations. The increase in the apparent interfacial resistance has then to be ascribed to another process than interface-related phenomena. The progressive disordering of the transition metals in the bulk structure of the active material upon cycling [47,48] cannot explain the difference of behavior as it is most probably occurring in the bulk of LMN-1 and LMN-4, independently of the active material surface history. A reasonable interpretation could be the deterioration of the composite electrode coming from a contact loss between active material grains and carbon black electrical network due to mechanical constraints. It is also possible that subtle changes in composition occur in the interphase in a way that changes the ion transport properties through the surface layer. In order to test the contact issue hypothesis, additional EIS experiments have been done after 20 cycles in the reduced state for both materials. Electrodes were removed from the cell, pressed under 3 tons and put in a new cell with fresh electrolyte. Very little effect can be seen in the case of LMN-4 (Fig. 5a) as the overall resistance measured goes from 45 to 37 Ω after being pressed. The same experiment in the case of LMN-1 had a more drastic effect on the values of the resistance, decreasing from 160 to 120 Ω (Fig. 5b). These results show in particular that the LMN-1 electrode suffered from defective electronic contact between grains or between active material grains and carbon black particles, as opposed to the LMN-4 case and therefore, contributing to the significant increase of the overall observed resistance. This contribution is not clearly observed or stays small in the case of LMN-4 although its contribution cannot completely be ruled out. In short, the deterioration upon cycling of Ar-stored LMN-1 performance is not due to the building of some interphase, but is due on the contrary to other phenomenon such as electric contact loss within the composite electrode framework.

In summary, our results show that the same material has a different electrochemical behavior and a different interface evolution as a function of the surface chemistry and/or amount of pristine surface layer. It has been already observed by several authors that surface modification has a strong consequence on the further electrochemical behavior, and more specifically on the capacity retention upon cycling [25,49–51]. In the present study, the origin of such drastic difference in the electrochemical behavior lies in the presence or absence of a pristine Li_2CO_3 layer leading to different evolutions of surface chemistry after reaction with electrolyte species upon immersion in the liquid electrolyte. Such behavior is in agreement with the studies of Dahn et al. [52,53] on $LiCoO_2$.

4.2. Relationships between amount of interphase and performance

We discuss now the influence of the amount of interphase (determined from ^{7}Li NMR intensity at the end of discharge) on the electrochemical performance. For LMN-4, the electrolyte-reacted Li_2CO_3 layer leads to the building of a thick interphase at the end of the 5th discharge (1000 a.u., see Fig. 6g), which is correlated to low capacity (Fig. 1) and large polarization (Fig. 2). At further cycles, the amount of interphase decreases (400 a.u.), the capacity slightly increases, and the polarization partly decreases. For LMN-1 during the first cycles (i.e. before any deterioration of the composite electrode framework occurs), a much lower amount of interphase is comparatively measured (100 a.u., see Fig. 6h), together with higher capacity (Fig. 1) and lower polarization (Fig. 2). Such observations lead us to conclude that a too high amount of surface species is detrimental to the performance.

In the following we compare the amount of interphase, the interfacial resistance and the performance evolution for both compounds after 20 cycles. For LMN-4, a moderate amount of interphase (400 a.u., see Fig. 6g and i) correlates with low interfacial resistance and stabilized capacity. For LMN-1, a very low amount of interphase (100 a.u., see Fig. 6h and j) correlates with high interfacial resistance coming from electrode degradation, and still decreasing capacity. In the former case, a moderate amount of interphase plays a beneficial role on the long term performance, while in the latter case an insufficient amount of interphase is detrimental to the performance stabilization. Thus, some minimum amount of interphase (coming for instance from surface side reactions with the electrolyte) seems to be needed and seems to play the role of cement to help maintaining physical contact between grains as no significant degradation of the electrical contact within the electrode could be observed by EIS for the material stored in air compared to that stored under argon atmosphere.

In summary, the amount of interphase was proved to influence drastically the electrochemical performance. A too large amount or an insufficient amount of surface species is detrimental to the performance, while a moderate amount of interphase plays a beneficial role on the long term performance. A minimum amount of interphase seems to be required to play the role of cement or binder to help maintaining electrode integrity upon volume variations occurring on cycling. These results emphasize the complexity of the interphase structure and the fact that its evolution cannot be described by a simple model.

5. Conclusions

Different electrochemical behaviors were observed for $LiNi_{0.5}Mn_{0.5}O_2$ samples depending of the atmosphere of storage (air versus argon) and independently of their synthesis route and specific surface areas. These behaviors can be linked to a different type of pristine interphase and in particular to the presence of initial Li_2CO_3 on the surface of air-stored samples, compared to a virgin surface of Ar-stored samples.

Samples stored in air exhibit a rapid specific capacity loss during the first cycles and reach then stabilization from the 5th cycle on. On the contrary, samples stored in argon display less stability and show a progressive capacity loss along the 20 first cycles. Surface evolution along the electrochemical cycling, as probed by ex situ ^{7}Li MAS NMR, EIS and XPS is also different depending on the storage atmosphere of pristine samples. In addition, XPS results suggest that organic species have a tendency to cover lithiated inorganic species formed on the surface of the grains of active material.

Careful comparison of surface phenomena (followed by Li NMR intensity, EIS interfacial resistance, and XPS) and electrochemical bulk properties (total capacity, and overall kinetics obtained from polarization) along cycling lead us to draw important conclusions on the relationships between surface chemistry and electrochemical behavior. For air-stored $LiNi_{0.5}Mn_{0.5}O_2$ sample, the overall electrochemical behavior is fully driven by surface phenomena. On the contrary, for Ar-stored $LiNi_{0.5}Mn_{0.5}O_2$ sample, the performance fading upon cycling is not due to interphase phenomena, but comes from other phenomenon such as electric contact loss within the composite electrode framework. The low amount of surface species and their progressive removal along the continuous decrease of performances suggested that surface species is needed to some extend to protect the electrode from degradation.

Finally, comparing quantitative surface evolution and performance for the materials initially stored in air or in protected atmosphere suggests that an appropriate amount of interphase would lead to a compromise between resistive and protective properties of the interphase and therefore between high specific capacity and long term stability upon cycling. On the contrary, a too large amount or an insufficient amount of surface species is detrimental to good cycling performance. Nevertheless, for these materials, the presence of a pristine surface layer leads to a performance stabilization upon the first cycles and the exposure of the material to atmosphere is clearly not detrimental.

Such highly important considerations on the relationships between surface chemistry, amount of interphase, electrochemical behavior and performance had never been highlighted before.

Acknowledgements

The authors wish to thank Dr. Danielle Gonbeau and Dr. Remi Dedryvère for helpful discussion on XPS analysis. Financial support of the Ph.D. of Jean-Frédéric Martin from the Region Pays de la Loire is gratefully acknowledged.

Appendix A. Supplementary data

Supplementary data associated with this article can be found, in the online version, at doi:10.1016/j.jpowsour.2010.07.049.

References

[1] B. Scrosati, J. Electrochem. Soc. 139 (1992) 10.
[2] K.G. McColl, J. Power Sources 48 (1994) 29.
[3] X. Zhang, P.N. Ross, R. Kostecki, F. Kong, S. Sloop, J.B. Kerr, K. Striebel, E.J. Cairns, F. McLarnon, J. Electrochem. Soc. 148 (2001) A463.
[4] K. Amine, J. Liu, ITE Lett. 1 (2000) 59.
[5] Y. Makimura, T. Ohzuku, J. Power Sources 156 (2003) 119.
[6] Z. Lu, L.Y. Beaulieu, R.A. Donaberger, C.L. Thomas, J.R. Dahn, J. Electrochem. Soc. 149 (6) (2002) A778.
[7] W.-S. Yoon, Y. Paik, X.Q. Yang, M. Balasubramanian, J. McBreen, C.P. Grey, Electrochem. Solid-State Lett. 5 (11) (2002) A263.
[8] C.S. Johnson, J.S. Kim, A.J. Kropf, A.J. Kahaian, J.T. Vaughey, L.M.L. Fransson, K. Edström, M.M. Thackeray, Chem. Mater. 15 (12) (2003) 2313.
[9] J. Bréger, N. Dupré, P.J. Chupas, P.L. Lee, T. Proffen, J.B. Parise, C.P. Grey, J. Am. Chem. Soc. 127 (20) (2005) 7529.
[10] H.H. Li, N. Yabuuchi, Y.S. Meng, S. Kumar, J. Bréger, C.P. Grey, S.H. Yang, Chem. Mater. 19 (10) (2007) 2551.
[11] Y. Hinuma, Y.S. Meng, K. Kang, G. Ceder, Chem. Mater. 19 (7) (2007) 1790.
[12] J. Bréger, M. Jiang, N. Dupré, Y.S. Meng, S.H. Yang, G. Ceder, C.P. Grey, J. Solid State Chem. 178 (9) (2005) 2575.
[13] A. Andersson, B. Kalska, L. Häggström, J.O. Thomas, Solid State Ionics 130 (1–2) (2000) 41.
[14] R. Dominko, J.M. Goupil, M. Bele, M. Gaberscek, M. Remskar, D. Hanzel, J. Jamnik, J. Power Sources 153 (2006) 274.
[15] K. Striebel, J. Shim, V. Srinivasan, J. Newman, J. Electrochem. Soc. 152 (4) (2005) A664.
[16] K.G. Chen, X. Song, T.J. Richardson, J. Electrochem. Soc. 154 (7) (2007) A627.
[17] K. Zaghib, A. Mauger, J.B. Goodenough, F. Gendron, C.M. Julien, Chem. Mater. 19 (15) (2007) 3740.
[18] J.D. Wilcox, M.M. Doeff, M. Marcinek, R. Kostecki, J. Electrochem. Soc. 154 (5) (2007) A389.
[19] B. Ellis, W.H. Kan, W.R. Makahnouk, L.F. Nazar, J. Mater. Chem. 17 (30) (2007) 3248.
[20] L. Wang, Y. Huang, R. Jiang, D. Jia, Electrochim. Acta 52 (54) (2007) 6778.
[21] K. Amine, M.J. Hammond, J. Liu, C. Chen, D.W. Dees, A.N. Jansen, G.L. Henriksen, Abstract 332, the 10th international meeting on lithium batteries, Como, Italy, May 28 to June 2, 2000.
[22] E. Peled, J. Electrochem. Soc. 126 (1979) 2047.
[23] D. Aurbach, B. Markovsky, M.D. Levi, E. Levi, A. Schechter, M. Moshkovich, Y. Cohen, J. Power Sources 81–82 (1999) 95.
[24] S.S. Zhang, K. Xu, T.R. Jow, Electrochem. Solid-State Lett. 5 (5) (2002) A92.
[25] D Aurbach, B. Markovsky, G. Salitra, E. Markevitch, Y. Talyossef, M. Koltypin, L. Nazar, B. Ellis, D. Kovacheva, J. Power Sources 165 (2) (2007) 491.
[26] K. Edström, T. Gustafsson, J.O. Thomas, Electrochim. Acta 50 (2–3) (2004) 397.
[27] Y. Sundarayya, S.K.C. Kumara, C.S. Sunandana, Mater. Res. Bull. 42 (11) (2007) 1942.
[28] D. Aurbach, M.D. Levi, E. Levi, H. Teller, B. Markovsky, G. Salitra, U. Heider, L. Heider, J. Electrochem. Soc. 145 (9) (1998) 3024.
[29] E. Ericksson, PhD Thesis, Uppsala University, 2001.
[30] T. Matsushita, K. Dokko, K. Kanamura, J. Electrochem. Soc. 152 (11) (2005) A2229.
[31] H. Ota, T. Akai, H. Namita, S. Yamaguchi, M. Nomura, J. Power Sources 119–121 (2003) 567.
[32] B.J. Neudecker, R.A. Zuhr, B.S. Kwak, J.B. Bates, J.D. Robertson, J. Electrochem. Soc. 145 (12) (1998) 4148.
[33] J.C. Dupin, D. Gonbeau, H. Benqlilou-Moudden, Ph. Vinatier, A. Levasseur, Thin Solid Films 384 (2001) 23.
[34] M. Ménétrier, C. Vaysse, L. Croguennec, C. Delmas, C. Jordy, F. Bonhomme, P. Biensan, Electrochem. Solid State Lett. 7 (6) (2004) A140.
[35] B. Meyer, N. Leifer, S. Sakamoto, S. Greenbaum, C.P. Grey, Electrochem. Solid-State Lett. 8 (3) (2005) A145.
[36] N. Dupré, J.-F. Martin, D. Guyomard, A. Yamada, R. Kanno, J. Mater. Chem. 18 (2008) 4266.
[37] N. Dupré, J.-F. Martin, J. Oliveri, D. Guyomard, A. Yamada, R. Kanno, Electrochem. Commun. 10 (12) (2008) 1897.
[38] N. Dupré, J.-F. Martin, D. Guyomard, A. Yamada, R. Kanno, J. Electrochem. Soc. 156 (5) (2009) C180.
[39] S. Gopukumar, K.Y. Chung, K.B. Kim, Electrochim. Acta 49 (2004) 803.
[40] M. Yoncheva, R. Stoyanova, E. Zhecheva, R. Alcántara, G. Ortiz, J.L. Tirado, Electrochim. Acta 54 (2009) 1694.
[41] M. Koltypin, D. Aurbach, L. Nazar, B. Ellis, Electrochem. Solid State Lett. 10 (2) (2007) A40.
[42] V. Eshkenazi, E. Peled, L. Burstein, D. Golodnitsky, Solid State Ionics 170 (2004) 83.
[43] A. Anderson, Surface Phenomena in Li-ion Batteries, Comprehensive Summaries of Uppsala Dissertations from the Faculty of Science and Technology, A.U. Uppsaliensis Editor, Uppsala, 2001.

[44] A.M. Andersson, M. Herstedt, A. Bishop, K. Edström, Electrochim. Acta 47 (2002) 1885.
[45] G. Zhuang, Y. Chen, Langmuir 15 (1999) 1470.
[46] L.J. Rendeck, G.S. Chottiner, J. Electrochem. Soc. 149 (2002) E408.
[47] H. Li, H. Hayley, N. Yabuuchi, Y.S. Meng, S. Kumar, J. Bréger, C.P. Grey, S.H. Yang, Chem. Mater. 19 (10) (2007) 2551.
[48] J. Bréger, Y.S. Meng, Y. Hinuma, S. Kumar, K. Kang, S.H. Yang, G. Ceder, C.P. Grey, Chem. Mater. 18 (20) (2006) 4768.
[49] D. Aurbach, K. Gamolsky, B. Markovsky, G. Salitra, Y. Gofer, U. Gofer, U. Heider, R. Oesten, M. Schmidt, J. Electrochem. Soc. 147 (2000) 1322.
[50] M. Koltypin, D. Aurbach, L. Nazar, B. Ellis, J. Power Sources 174 (2008) 1241.
[51] M. Kerlau, R. Kostecki, J. Electrochem. Soc. 153 (2006) A1644.
[52] Z. Chen, J.R. Dahn, Electrochim. Acta 49 (2003) 1079.
[53] Z. Chen, J.R. Dahn, Electrochem. Solid State Lett. 7 (19) (2004) A11.